Journal of Control, Automation and Electrical Systems (2019) 30:1019–1029
https://doi.org/10.1007/s40313-019-00510-w

Adaptive and Exact Linearization Control of Multicellular Power Converter Based on Shunt Active Power Filter

Boubakeur Rouabah[1] · Lazhar Rahmani[1] · Houari Toubakh[2] · Eric Duviella[2]

Received: 17 January 2019 / Revised: 18 July 2019 / Accepted: 17 August 2019 / Published online: 27 August 2019

Abstract
Most research work on active power filter (APF) uses constant DC bus voltage. However, variable nonlinear load might affect the stability of these APFs and increase the power switching loss and voltage stress on switches. In this work, the contribution is twofold. First, regulate the DC bus voltage of APF, adaptively, with the nonlinear load variations and generate the reference of the harmonic currents based on the instantaneous power theory. Second, track this reference to mitigate harmonics of the grid-side current by the exact linearization control of three-phase multicellular power converter with reduced rating power switches and reduced power switching loss under variable nonlinear load. Simulation results with comparison study with classical topology of power converter demonstrate that the adaptive exact linearization control enhances the power quality with a minimum power switching loss and reduces the total harmonic distortion of grid-side current to a value that satisfies the limits of IEEE standard. Moreover, the DC bus voltage changes, adaptively, according to different values of nonlinear load power.

Keywords Shunt active power filter (SAPF) · Multicellular power converter · Adaptive exact linearization control · Variable DC bus voltage

List of symbols

v_s	(a, b, c) three-phase voltage grid
i_s	(a, b, c) three-phase current grid
i_L	(a, b, c) three-phase current load
i_f	(a, b, c) three-phase current filter
V_{dc}	DC bus voltage
C_{dc}	DC bus capacitor
v_C	Flying capacitor voltage
C	Flying capacitor value
i_C	Flying capacitor current
R_f	Filter resistor
L_L	Load inductor
L_f	Filter inductor
S	Switching function
P	Active power
q	Reactive power
E_{dc}	DC bus energy
Kr	Proportional regulator
$1/s$	Integrator
R_L	Nonlinear load resistor
ε_s	Static error
φ_s	Phase angle between grid side voltage and current

✉ Boubakeur Rouabah
boubakeurrouabah@yahoo.fr

Lazhar Rahmani
lazhar_rah@yahoo.fr

Houari Toubakh
houari.toubakh@mines-douai.fr

Eric Duviella
eric.duviella@imt-lille-douai.fr

[1] Automatic Laboratory, Department of Electrical Engineering, Ferhat Abbas University, 19000 Sétif, Algeria

[2] IMT Lille Douai, Univ. Lille, URIA, 59000 Lille, France

1 Introduction

In recent years, the power quality of electrical distribution systems has become a significant issue due to the widespread use of controlled power converters or variable nonlinear loads in domestic (computers, uninterruptible power supply, etc.) or industrial installations (high voltage levels such as arc furnace, adjustable speed drive, etc.). To solve this issue and enhance the power quality, active power filters (APFs)

based on two-level power converter with high and constant DC bus voltage have been designed. However, they present some drawbacks that are caused to the dv/dt voltage stress of power electronic switches and switching loss increase with the increment of DC bus voltage. Therefore, it is still necessary for APF to improve the power quality. Solutions based on multilevel power converter and variable DC bus voltage have been proposed in Yao et al. (2016); Ray et al. (2018); Martinez-Rodriguez et al. (2017). In addition, nonlinear loads absorb non-sinusoidal currents producing harmonic pollution in the power grid, that can affect the equipment connected in the same power grid by excessive heating in electrical machinery, magnetic interference and low power factor and can cause noise in communication circuit (Chang et al. 2013; Yu et al. 2018; Alexandre et al. 2018).

Traditional solutions based on passive LC filters have been used to avoid these undesirable effects (Mahanty and Kapoor 2008; Wu et al. 2005; Sakar et al. 2017). However, they cannot deal with variations of the power grid characteristic, resonance with LC loads and large size systems (Karuppanan and Mahapatra 2014). It is the main reason why several APF topologies have been recently designed benefiting to progress in power electronics devices. These solutions are adjustable and overcome the problems of harmonics and power quality. They have the advantage to adapt the parameters of the APF according to nonlinear load variations (Antunes et al. 2018; Mesbahi et al. 2014).

Moreover, they are classified based on their topologies (series, shunt and hybrid) and their types of power converter (Belaidi et al. 2011). The series APF are connected with power grid through coupling transformer and are used to compensate the voltage harmonics; the shunt APF (SAPF) is connected in parallel with the nonlinear load (Mekri et al. 2010; Litrán and Salmerón 2017; Roldán-Pérez et al. 2017). The power converter in SAPF operates as current source by injecting currents equal, but opposite to the harmonic of nonlinear load currents. It aims at reducing the total harmonic distortion (THD) of grid-side currents, compensates reactive power, and leads to a power factor close to the unity (Chaoui et al. 2010; Ouchen et al. 2016; Hoseinpour et al. 2012). The performance of SAPF is not only based on the power converter parameters, but also on the control method and on the current reference synthesis method (Bouzelata et al. 2015). Many topologies and methods have been suggested in the literature to realize and control SAPF. Two-level converter topology is more and more used in SAPF (Zafari and Jazaeri 2016; Kale and Özdemir 2005; Chen et al. 2010; Zhao et al. 2009; Ait Chihab et al. 2016). In Chaoui et al. (2010); Mesbahi et al. (2014), the direct power control for SAPF with two-level converter offers sinusoidal grid current and low THD for both ideal and distorted grid voltages. In Hoseinpour et al. (2012), the SAPF is used to eliminate current harmonics in wind energy system. In Bouzelata et al. (2015); Belaidi et al. (2011), a SAPF feed by solar panels can assure both power quality enhancement and solar power injection in the grid. However, a classical two-level converter topology means a high voltage stress on power electronic switches, a high dv/dt ratio and considerable THD of grid-side current (Colak et al. 2011). It is the reason why, in high power application and variable nonlinear load, a SAPF with multilevel topology of power converter is used. In Singh et al. (2017); Lee and Heng (2017); Chebabhi et al. (2016); Babaei and Hosseini (2009); Taallah and Mekhilef (2014), multilevel power converters with low voltage stress and low power switches have been applied to generate more levels of output voltage and low harmonic content in grid-side current. It reduces the electromagnetic compatibility problems and power losses in power electronic switches. Moreover, the multicellular power converters have the advantage to operate with high DC bus voltage, low power loss and low voltage stress in power electronic switches and the DC bus voltage being divided on flying capacitors naturally (Sadigh et al. 2016; Meynard et al. 2002; Defaÿ et al. 2008). In Gateau (1997); Bensaid (2001); Olivier (1998), a multicellular power converter with exact linearization demonstrates good tracking of capacitor voltage reference and load current with acceptable static error and time response. In Defaÿ et al. (2008), a predictive control without voltage sensors of multicellular converter in SAPF shows low THD and power quality enhancement of grid in both balanced and unbalanced loads. In Aourir et al. (2018), a flatness-based control of multicellular converter with SAPF for power quality improvement has been designed. A direct control of four-leg four-level multicellular converter with SAPF using a table calculated offline to give appropriate control can enhance power quality as investigated in Fadel et al. (2012). However, when using SAPF, the stability of DC bus voltage at the optimal value is very important. Low DC bus voltage cannot enhance the power quality as required, and high DC bus voltage increases the switching loss (Liu et al. 2014). Moreover, as the nonlinear load power varies from time to time, the SAPF with constant DC bus voltage can inject only a fixed reactive power (Lam and Wong. 2014). Therefore, the use of SAPF with DC bus voltage that changes adaptively with nonlinear load power is very important. In Lam and Wong (2014), simulation and experimental results of three-phase four-wire center-split hybrid APF with two-level topology are presented. The effectiveness of the proposed adaptive DC bus voltage control in dynamic reactive power compensation to reduce switching loss and switching noise is verified. In this paper, we propose a new topology of a SAPF to collect all advantages of linearization exact control, multicellular topology of power converter, adaptive DC bus voltage control to enhance power quality in high DC bus voltage and variable nonlinear load. The theoretical study is validated through simulation using MATLAB/SIMULINK.

For a better understanding of the important effects of variable DC bus voltage and multicellular topology in SAPF, we propose:

- The use of SAPF and power quality improvement based on multicellular topology in variable nonlinear loads connected to the power grid and high DC bus voltage.
- To regulate the DC bus voltage at the optimum value to achieve a minimum switching loss and low voltage stress in power electronic switches.
- The exact linearization control for multicellular power converter to obtain a THD of grid-side currents less than 5% and compile with harmonic current standards (IEEE-519).

The structure of this paper is as follows: Section 2 describes the power circuit of SAPF with three-phase multicellular power converter. The modeling of the proposed SAPF is presented in Sect. 3, and the DC bus voltage regulation with instantaneous power theory is introduced in Sect. 4. The exact linearization control of three-phase multicellular power converter is given in Sect. 5. Finally, the simulation results and conclusions of this research are discussed in Sects. 6 and 7, respectively.

2 System descriptions

Figure 1 shows the power circuit of a three-phase SAPF based on multicellular power converter. In this system, the grid is considered ideal. Consequently, the multicellular power converter supplies the current harmonic and reactive component to make the grid-side current sinusoidal and to obtain a unity power factor in the power grid.

As shown in Fig. 1, the multicellular power converter topology is based on the connection in series of three commutation cells. Each cell is composed by a flying capacitor (C_{k1}, C_{k2}) and two power switches (S_{1k}, $\bar{S}_{1k}$) with complementary discrete control (if one switch is open ($S_{1k} = 0$), the other switch is close ($\bar{S}_{1k} = 1$). To divide the constraint of DC bus voltage (V_{dc}) per 3 in power switches, the control law balances the flying capacitor voltages at desired values ($V_{C_{k1}} = \frac{V_{\mathrm{dc}}}{3}$, $V_{C_{k2}} = \frac{2V_{\mathrm{dc}}}{3}$) and generates four levels in output voltage.

Table 1 shows how the output voltage levels in one phase of multicellular converter are generated.

3 Modeling of three-phase four-level multicellular power converter

The currents in the floating capacitors for three-phase multicellular power converter are given by Eqs. (1) and (2)

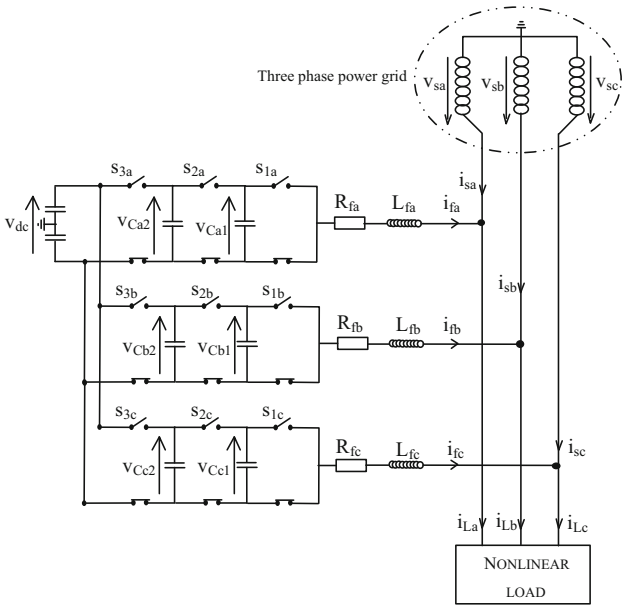

Fig. 1 Proposed shunt active power filter

Table 1 Output voltage levels of multicellular converter

Output voltage levels	$(S_{1i}\ S_{2i}\ S_{3i})$
$\frac{-V_{\mathrm{dc}}}{2}$	(0 0 0)
$\frac{-V_{\mathrm{dc}}}{6}$	(1 0 0), (0 1 0), (0 0 1)
$\frac{V_{\mathrm{dc}}}{6}$	(1 1 0), (0 1 1), (1 0 1)
$\frac{V_{\mathrm{dc}}}{2}$	(1 1 1)

(Gateau. 1997), where $k = [a, b, c]$, $i = [1, 2]$. The voltage drop in the power grid impedance is neglected.

$$\dot{i}_{C_{ki}} = C_{ki}\frac{\mathrm{d}}{\mathrm{d}t}v_{C_{ki}} \tag{1}$$

$$\frac{\mathrm{d}}{\mathrm{d}t}v_{C_{ki}} = \frac{1}{C_{ki}}[S_{(i+1)k} - S_{ik}]i_{fk} \tag{2}$$

The current filter variations are given in Eqs. (3) and (4):

$$L_{fk}\frac{\mathrm{d}i_{fk}}{\mathrm{d}t} = S_{1k}\left[v_{C_{k1}}\right] + S_{2k}\left[v_{C_{k2}} - v_{C_{k1}}\right] + S_{3k}\left[v_{\mathrm{dc}} - v_{C_{k2}}\right] - R_{fk}i_{fk} - \frac{v_{\mathrm{dc}}}{2} - v_{sk} \tag{3}$$

$$i_{fk} = i_{Lk} - i_{sk} \tag{4}$$

According to Eqs. (2), (3) and (4), a nonlinear (coupled) state representation of three-phase SAPF with four-level multicellular power converter is given in Eq. (5). This nonlinearity is observed in the relation between the switching functions

(S_{1k}, S_{2k}, S_{3k}) and $(\frac{d}{dt}v_{Ck1}, \frac{d}{dt}v_{Ck2}, \frac{d}{dt}i_{fk})$. A linear relation links between $(v_{Ck1}, v_{Ck2}, i_{fk})$ and $(\frac{d}{dt}v_{Ck1}, \frac{d}{dt}v_{Ck2}, \frac{d}{dt}i_{fk})$.

$$\begin{bmatrix} \frac{d}{dt}v_{Ck1} \\ \frac{d}{dt}v_{Ck2} \\ \frac{d}{dt}i_{fk} \end{bmatrix} = \begin{bmatrix} 0\,0 & 0 \\ 0\,0 & 0 \\ 0\,0 & \frac{-R_{fk}}{L_{fk}} \end{bmatrix} \begin{bmatrix} v_{Ck1} \\ v_{Ck2} \\ i_{fk} \end{bmatrix} + \begin{bmatrix} \frac{-(i_{Lk}-i_{sk})}{C} & \frac{(i_{Lk}-i_{sk})}{C} & 0 \\ 0 & \frac{-(i_{Lk}-i_{sk})}{C} & \frac{(i_{Lk}-i_{sk})}{C} \\ \frac{v_{Ck1}}{L_{fk}} & \frac{v_{Ck2}-v_{Ck1}}{L_{fk}} & \frac{v_{dc}-v_{Ck2}}{L_{fk}} \end{bmatrix} \times \begin{bmatrix} S_{1k} \\ S_{2k} \\ S_{3k} \end{bmatrix} + \begin{bmatrix} 0 \\ 0 \\ \frac{-v_{\mathrm{dc}}}{2L_{fk}} - \frac{v_{sk}}{L_{fk}} \end{bmatrix} \tag{5}$$

4 DC bus voltage regulation and filter current reference generation

To regulate the DC bus voltage at a desired value, to compensate the reactive power and to generate the current filter references, there are several control techniques published in the literature. In this paper, we use instantaneous power theory proposed by Akagi (Zafari and Jazaeri. 2016). This theory is detailed in (Kale and Özdemir. 2005).

The instantaneous values of the active and reactive power in $\alpha\beta$ frame are expressed by Eqs. (6) and (7) as follows:

$$p(t) = V_{s\alpha} \cdot i_{L\alpha} + V_{s\beta} \cdot i_{L\beta} \tag{6}$$

$$q(t) = -V_{s\alpha} \cdot i_{L\beta} + V_{s\beta} \cdot i_{L\alpha} \tag{7}$$

So the nonlinear load currents are given by:

$$\begin{bmatrix} i_{L\alpha} \\ i_{L\beta} \end{bmatrix} = \frac{1}{V_{s\alpha}^2 + V_{s\beta}^2} \begin{bmatrix} V_{s\alpha} & V_{s\beta} \\ V_{s\beta} & -V_{s\alpha} \end{bmatrix} \begin{bmatrix} p(t) \\ q(t) \end{bmatrix} \tag{8}$$

The instantaneous active and reactive powers can be expressed by Eqs. (9) and (10) (Kale and Özdemir 2005):

$$p(t) = \bar{P} + \tilde{P} \tag{9}$$

$$q(t) = \bar{q} + \tilde{q} \tag{10}$$

where $\bar{P}$: DC component of the instantaneous power $p(t)$, $\tilde{P}$: AC component of the instantaneous power $p(t)$, $\bar{q}$: DC component of the instantaneous reactive power $q(t)$, $\tilde{q}$: AC component of the instantaneous reactive power $q(t)$.

The main objectives of the SAPF in this work are:

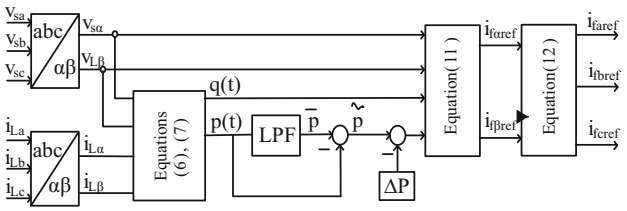

Fig. 2 Instantaneous power theory

a. In steady state: to compensate the consumed reactive energy, to eliminate harmonics caused by nonlinear load and to track the reference with low oscillations and zero static error ε_s, which means also to have a sinusoidal current source ($\mathrm{THD}_s \approx 0\%$), in phase with the grid-side voltage $\varphi_s \approx 0$, and good regulation of the DC bus voltage $\varepsilon_s \approx 0$.
b. In transient state: to have a quick response with low overshoot to sudden external conditions for both load variations and DC bus voltage changes (rejected disturbance).

The reference filter currents in αβ frame are given in Eq. (11)

$$\begin{bmatrix} i_{f\alpha\mathrm{ref}} \\ i_{f\beta\mathrm{ref}} \end{bmatrix} = \frac{1}{V_{s\alpha}^2 + V_{s\beta}^2} \begin{bmatrix} V_{s\alpha} & V_{s\beta} \\ V_{s\beta} & -V_{s\alpha} \end{bmatrix} \begin{bmatrix} \tilde{P} - \Delta P \\ \bar{q} + \tilde{q} \end{bmatrix} \tag{11}$$

where ΔP is the active power necessary to regulate DC side voltage at a given reference.

The reference of the filter currents in a, b, c frame is given by Eq. (12):

$$\begin{bmatrix} i_{f\alpha\mathrm{ref}} \\ i_{f\beta\mathrm{ref}} \\ i_{f\mathrm{cref}} \end{bmatrix} = \sqrt{\frac{2}{3}} \begin{bmatrix} 1 & 0 \\ \frac{-1}{2} & \frac{\sqrt{3}}{2} \\ \frac{-1}{2} & \frac{-\sqrt{3}}{2} \end{bmatrix} \begin{bmatrix} i_{f\alpha\mathrm{ref}} \\ i_{f\beta\mathrm{ref}} \end{bmatrix} \tag{12}$$

The instantaneous power theory is represented in Fig. 2. To extract the AC component of active power ($\tilde{p}$), a second-order low-pass filter (LPF) is used with the following expression of transfer function $\frac{\omega_0^2}{s^2+2\delta\omega_0+\omega_0^2}$, with $\omega_0 = 2\pi f_0$, where $f_0 = 40$ Hz is the cutoff frequency, $\delta = 0.707$ is the damping factor.

4.1 Calculation of ΔP

The reference energy of the DC bus side can be expressed by Eq. (13):

$$E_{\mathrm{dcref}} = \frac{1}{2} C_{\mathrm{dc}} V_{\mathrm{dcref}}^2 \tag{13}$$

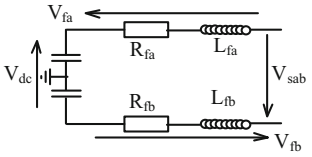

Fig. 3 Relation between DC voltage and phase-to-phase grid voltage v_{sab}

The instantaneous energy of the DC bus side can be expressed by Eq. (14):

$$E_{\mathrm{dc}}(t) = \frac{1}{2} C_{\mathrm{dc}} v_{\mathrm{dc}}^2 \tag{14}$$

The difference between the reference energy and the instantaneous energy is given in Eq. (18).

$$\Delta E_{\mathrm{dc}} = \frac{C_{\mathrm{dc}}}{2}(V_{\mathrm{dcref}}^2 - v_{\mathrm{dc}}^2) \tag{15}$$

$$\Delta E_{\mathrm{dc}} = \frac{C_{\mathrm{dc}}}{2}(V_{\mathrm{dcref}} - v_{\mathrm{dc}})(V_{\mathrm{dcref}} + v_{\mathrm{dc}}) \tag{16}$$

$$V_{\mathrm{dcref}} - v_{\mathrm{dc}} = \Delta V_{\mathrm{dc}}$$

$$V_{\mathrm{dcref}} + v_{\mathrm{dc}} \cong 2V_{\mathrm{dcref}} \tag{17}$$

$$\Delta E_{\mathrm{dc}} \cong C_{\mathrm{dc}} V_{\mathrm{dcref}} \Delta V_{\mathrm{dc}} \tag{18}$$

The difference between the reference active power and the instantaneous active power ΔP of the capacity at the DC bus side, that is necessary to eliminate current harmonics and to compensate the reactive energy, is expressed by Eq. (19):

$$\Delta P = \frac{\Delta E_{\mathrm{dc}}}{\Delta t} \tag{19}$$

4.2 Calculation of V_{dcref}

To compensate the absorbed reactive power and harmonics caused by the nonlinear load, the multicellular power converter that acts as SAPF must inject a current into the power grid equal and in the opposite phase to the harmonic content of the grid-side currents. To achieve this condition, the DC bus reference voltage must be greater than the phase-to-phase voltage $V_{\mathrm{dcref}} > V_{\mathrm{sabmax}}$. If the active power of the nonlinear load increases, the $V_{\mathrm{dcref}} - V_{\mathrm{sabmax}}$ must be also increased to inject the necessary current as shown in Fig. 3. V_{sabmax} is a constant value. So, to increase the difference $V_{\mathrm{dc}} - V_{\mathrm{sabmax}}$, we must increase V_{dcref}.

The fundamental idea in this research work is that the reference voltage V_{dcref} of the DC bus must be varied adaptively with the variation of the nonlinear load power demand in order that the SAPF can inject the required compensation current. This current is used to eliminate the harmonics of grid-side current and to compensate the reactive power with minimum switching loss.

Therefore, the DC bus reference voltage V_{dcref} must be adapted with the variation of the nonlinear load, by considering $R_{fa} = R_{fb}$, $L_{fa} = L_{fb}$, $V_{fa} = V_{fb}$. Then, according to Fig. 3, the worst case is when the grid-side voltage is at the extreme value and the inverter must be able to supply the maximum compensation current. Therefore, the DC bus voltage is given by Eq. (20):

$$V_{\mathrm{dc}} = V_{\mathrm{sabmax}} + 2 * V_{fa} \tag{20}$$

If the nonlinear load current increases, the filter current increases. Consequently, V_{dcref} can be determined from current filter. Hence, we can calculate the minimum value of DC voltage by the following equation:

$$V_{\mathrm{dc(min)}} = V_{\mathrm{sabmax}} + 2L_f \frac{\Delta i_{\mathrm{famax}}}{\Delta t} + 2R_f i_{\mathrm{famax}} \tag{21}$$

V_{dc} can be determined from i_{famax} values. In this adaptive control, V_{dcref} values are determined from $|i_{\mathrm{fref}}|_{\mathrm{max}}$ value in one period (0.02 s) as follows:

- $|i_{\mathrm{fref}}|_{\mathrm{max}} < 8$ A, $V_{\mathrm{dcref}} = 1000$ V,
- $8\ \mathrm{A} \le |i_{\mathrm{fref}}|_{\mathrm{max}} < 13$ A, $V_{\mathrm{dcref}} = 1100$ V,
- $13\ \mathrm{A} \le |i_{\mathrm{fref}}|_{\mathrm{max}} < 18$ A, $V_{\mathrm{dcref}} = 1200$ V,
- $18\ \mathrm{A} \le |i_{\mathrm{fref}}|_{\mathrm{max}} < 23A$, $V_{\mathrm{dcref}} = 1300$ V,
- $23\ \mathrm{A} \le |i_{\mathrm{fref}}|_{\mathrm{max}}$, $V_{\mathrm{dcref}} = 1400$ V.

The V_{dcref} values (1000, 1100, 1200, 1300 and 1400) are determined by choosing the minimum V_{dcref} value that gives acceptable THD according to IEEE standard using MATLAB/SIMULINK.

5 Design of exact linearization control

The three-phase SAPF-based multicellular power converter with three-cell four-level output voltage given by the system Eq. (5) can be written in compact form as follows:

$$\frac{\mathrm{d}}{\mathrm{d}t}x = Fx + g(x)u + T \tag{22}$$

$$Y = x$$

$$\frac{\mathrm{d}}{\mathrm{d}t}Y = Fx + g(x)u + T \tag{23}$$

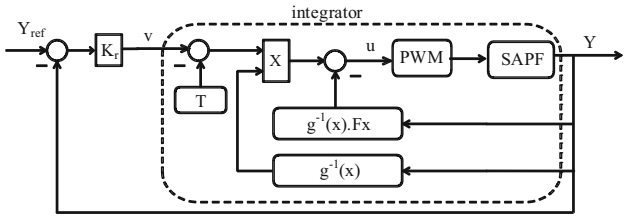

Fig. 4 Exact linearization control

where $x = [v_{Ck1}, v_{Ck2}, i_{fk}]^{\mathrm{T}}$ is the state vector, $Y_{\mathrm{ref}} = [V_{\mathrm{dc}}/3, 2V_{\mathrm{dc}}/3, i_{fk\mathrm{ref}}]$, the reference of state vector, and:

$$F = \begin{bmatrix} 0\,0 & 0 \\ 0\,0 & 0 \\ 0\,0 & \frac{-R_{fk}}{L_{fk}} \end{bmatrix}$$

$$g(x) = \begin{bmatrix} \frac{-(i_{Lk}-i_{sk})}{C} & \frac{(i_{Lk}-i_{sk})}{C} & 0 \\ 0 & \frac{-(i_{Lk}-i_{sk})}{C} & \frac{(i_{Lk}-i_{sk})}{C} \\ \frac{v_{Ck1}}{L_{fk}} & \frac{v_{Ck2}-v_{Ck1}}{L_{fk}} & \frac{v_{\mathrm{dc}}-v_{Ck2}}{L_{fk}} \end{bmatrix}$$

$u = [S_1, S_2, S_3]^{\mathrm{T}}$, the input vector,

$$T = \begin{bmatrix} 0 \\ 0 \\ \frac{-v_{dc}}{2L_{fk}} - \frac{v_k}{L_{fk}} \end{bmatrix}, \text{ a constant vector.}$$

Our objective is to find the input u and make the output Y very close to the desired value Y_{ref}, establishing a simple linear and direct relation between the control input u and the output Y. The idea consists of deriving the output Y until the input u appears in the derivative of the output (Chen et al. 2010). The derivative of the output Y is given by Eq. (23).

According to Eq. (23), the output Y is indirectly related to the input u. This input u appears in the first derivative of the output Y.

A new input control v which is equal to the derivative of the output Y is introduced and leads to the following equations (Gateau. 1997):

$$v = Fx + g(x)u + T \tag{24}$$

$$u = g^{-1}(x)[v - T] - g^{-1}(x)Fx \tag{25}$$

Finally, the exact linearization control given by Eq. (25) is represented in Fig. 4. Considering the proposed topology, the simplified scheme of exact linearization control in a closed loop with a proportional regulator $K_r = (K_{r1}\ K_{r1}\ K_{r2})$ is shown in Fig. 5, where K_{r1} is the proportional regulator for voltage closed loop, which regulates flying capacitor voltages V_{Ck1} and V_{Ck2}, and K_{r2} is the proportional regulator for current closed loop to regulate filter currents (i_f).

The closed-loop transfer function of system in flying capacitor voltages is equal to $\frac{1}{\tau_1 s+1}$, where $\tau_1 = \frac{1}{K_{r1}}$ is the time constant in voltage loop. The closed-loop transfer

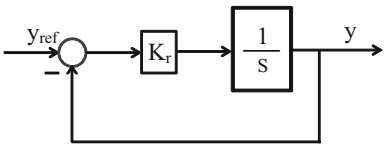

Fig. 5 Simplified scheme of the closed loop

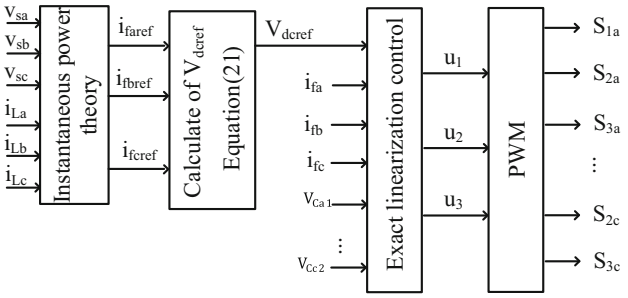

Fig. 6 Proposed control for the three-phase SAPF-based multicellular power converter

function of system in filter currents is equal to $\frac{1}{\tau_2 s+1}$, where $\tau_2 = \frac{1}{K_{r2}}$ is the time constant in current loop.

The time responses of first-order systems ($t_{r5\%} = 3\,\tau$) are supposed as follows:

- In voltage loop, to assure the rapidity of system we suppose $t_{r1} = 90 \times 10^{-3}$s; hence, $\tau_1 = 30 \times 10^{-3}$ s.
- The current loop must be rapid than voltage loop so we suppose $t_{r2} = 6 \times 10^{-4}$ s; hence, $\tau_2 = 2 \times 10^{-4}$ s.

Finally, to guarantee the stability of the system, the phase margin given by $\varphi_M = 180 + \varphi$, with $\varphi = \arg(K_r) - \arg(s)$, leads to $\varphi = 0 - 90$ involving $\varphi = -90$; $\varphi_M = 90 > 0$. Therefore, the system is stable with K_r values such as $K_{r1} = 34$, $K_{r2} = 5000$.

In Eq. (25), the control v is continuous and the control u is carried out based on a triangular signal (20 kHz) by pulse width modulation method (PWM) to have a binary signal (0, 1).

The global scheme of combined instantaneous power theory and adaptive exact linearization control of the three-phase shunt active power filter based on multicellular power converter with three-cell and four-level output voltage is represented in Fig. 6.

The instantaneous power theory generates the references of the filter current according to the nonlinear load power variations. If the nonlinear load power increases, the references of current filter increase (instantaneous power theory) and the adaptive control determines the appropriate value of V_{dcref}.

Therefore, the adaptive exact linearization control will adapt with the nonlinear load power variations.

Table 2 Design specification and circuit parameters

Switching frequency	$f_{sw} = 20$ kHz
Power grid frequency	50 Hz
The RMS phase-to-phase supply voltage	$V_S = 380$ V
DC bus voltage reference	$V_{dcref} = 1000$ V
Coupling filter impedance	$R_f = 1$ mΩ, $L_f = 13$ mH
Grid impedance	$R_s = 1$ mΩ, $L_s = 0.1\ 10^{-3}$ mH
Nonlinear load parameters	$R_L = 40\Omega$, $L_L = 10$mH
Proportional regulator	$K_{r1} = 34$ (voltage loop), $K_{r2} = 5000$ (current loop)
DC bus capacitor	$C_{dc} = 4000\mu$F
Flying capacitor of multicellular power converter	$C = 400\mu$F

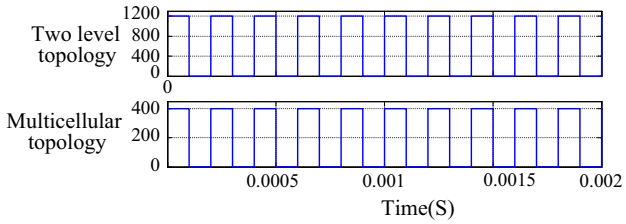

Fig. 7 Voltage stress on switches

6 Simulation results

To demonstrate the validity of the proposed control, some simulations are presented in this section. The instantaneous power theory combined with the adaptive exact linearization control is used to drive the three-phase SAPF-based multicellular power converter with three-cell and four-level output voltage as shown in Fig. 6. Simulation results are carried out using MATLAB/SIMULINK platform. The performances of the proposed control are evaluated in terms of THD of the grid-side current, the DC bus voltage regulation, and the reactive power compensation in both steady and transient states. The used parameters in the simulation are given in Table 2.

6.1 Improvement of switching stress and switching power loss

Figure 7 shows a comparison between voltage stress on switches of two-level power converter and voltage stress on switches of multicellular power converter with the same DC bus voltage $V_{dc} = 1200$ V and same switching frequency $f_{sw} = 50$ kHz.

According to Fig. 7, the voltage stress in two-level topology (1200 V) is three times higher than the proposed multicellular converter (400 V). This can prove the enhancement of voltage stress on switches of multicellular power converter.

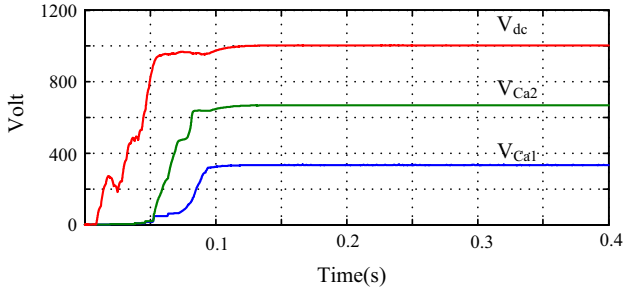

Fig. 8 DC bus voltage (V_{dc}) and flying capacitor voltages (V_{Ca1}, V_{Ca2})

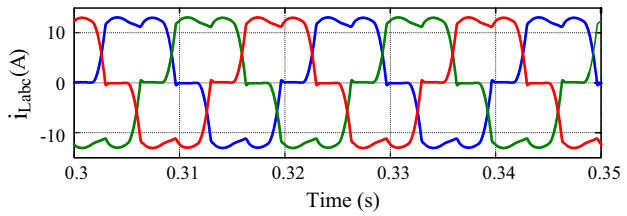

Fig. 9 Waveforms of the nonlinear load currents

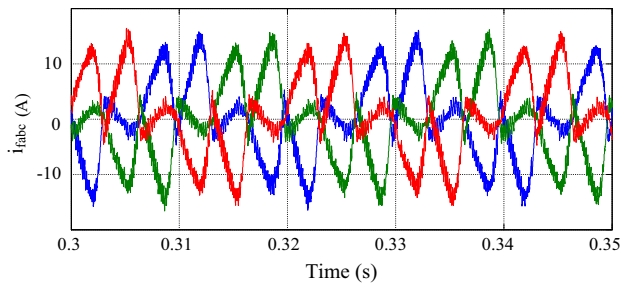

Fig. 10 Waveforms of the filter currents

Switching power losses are resulting from turn-on and turn-off process of power switches (IGBTs); these power losses are proportional to switching stress and switching frequency (Sadigh et al. 2016). So, for the same switching frequency and same DC bus voltage, the switching power losses in multicellular power topology are minimized. Moreover, in high voltage applications, two-level topology uses high-voltage IGBTs with augmented price and multicellular topology uses medium- or low-voltage IGBTs with lesser price.

6.2 Constant DC bus voltage and constant nonlinear load

The simulation results of combined instantaneous power theory and exact linearization control applied to SAPF based on multicellular power converter given in Figs. 8, 9, 10, 11, 12 and 13 have been obtained using MATLAB/SIMULINK. The nonlinear load is considered as three-phase diode rectifier with resistor $R_L = 40\ \Omega$ and inductor $L_L = 10$ mH in series.

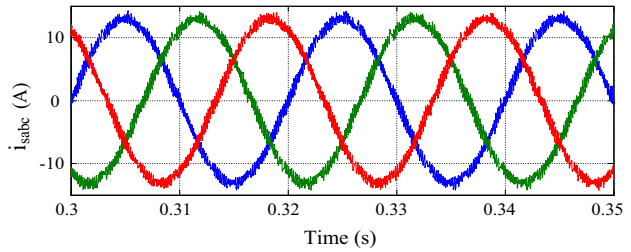

Fig. 11 Waveforms of the grid-side currents

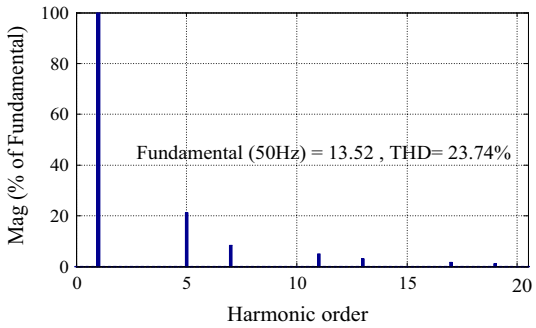

Fig. 12 THD of the nonlinear load currents

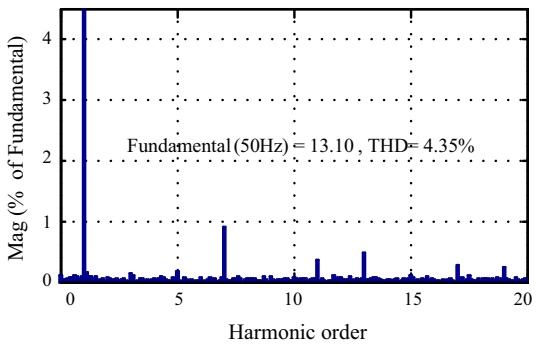

Fig. 13 THD of the grid-side currents

6.3 Steady-state performance

Figure 8 shows the DC bus voltage v_{dc} and flying capacitors voltages v_{Ca1} and v_{Ca2}. In steady state, the DC bus voltage v_{dc} tracks its reference $V_{dcref} = 1000$ V with static error $\varepsilon_s = 3$ V. The flying capacitor voltages v_{Ca1} and v_{Ca2} are very close to their references, $V_{ca1ref} = \frac{V_{dcref}}{3} = \frac{1000}{3} = 333.33$ V, $V_{ca2ref} = \frac{2\times V_{dcref}}{3} = \frac{2\times 1000}{3} = 666.66$ V.

The nonlinear load current as shown in Fig. 9 is totally deformed and can affect the power quality of the grid. Figure 12 gives the total harmonic distortion of nonlinear load current $THD_{iL} = 23.74\%$.

To improve the THD of the grid-side current and mitigate harmonics, Fig. 10 shows the filter current to be injected in the power grid. Figure 11 shows the waveforms of the grid-side current. It is clearly observed that the grid-side current is very close to the sinusoidal waveforms and in phase with the grid-side voltage. The corresponding spectrum is given in Fig. 13. The total harmonic distortion of the grid-side current is THD = 4.35% as shown in Fig. 13. It is very low compared to the nonlinear load current.

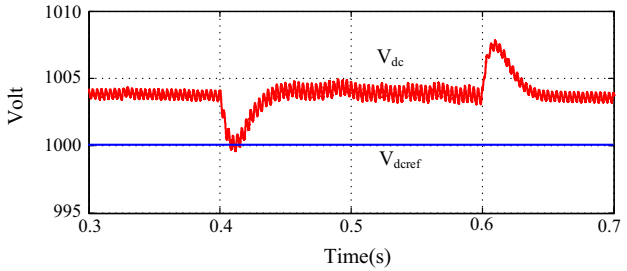

Fig. 14 Transient of the step change by increasing and decreasing nonlinear load power of 20% at $t = 0.4$ s and 0.6 s, respectively

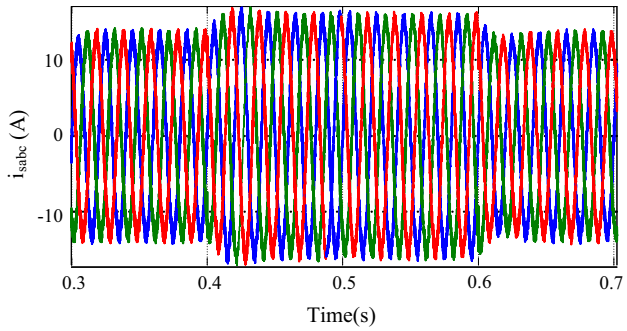

Fig. 15 The grid-side currents with increasing and decreasing the nonlinear load power of 20%

6.4 Transient-state performance

To demonstrate the robustness of the proposed topology, the control technique against the sudden changes in the nonlinear load and the DC bus voltage is described as follows:

6.4.1 Step change of the nonlinear load power

Figure 14 illustrates the transient of the step change by increasing and decreasing the nonlinear load power of 20% at $t = 0.4$ s and 0.6 s, respectively. Moreover, after a short transient, the DC bus voltage v_{dc} is maintained close to its reference value V_{dcref} with a good approximation and stability. The grid-side currents i_{sabc} have nearly sinusoidal waveforms and in phase with the input voltage as shown in Fig. 15. The corresponding transient values confirm that the v_{dc} is well kept with overshot of ± 4 V and time response of 0.06 s (about three cycles of the frequency line), and the static error is $\varepsilon_s = 4$ V. Although the linearized system is pure integrator, the static error is different from zero. This is due to the saturation MATLAB block that is used to generate the discrete PWM control.

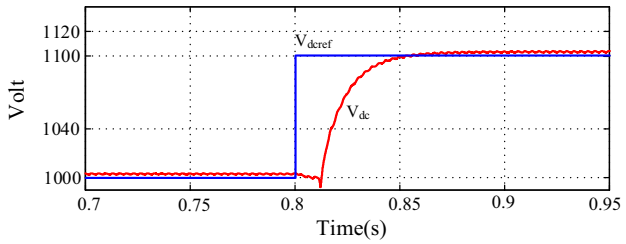

Fig. 16 V_{dc} and V_{dcref} with increasing V_{dcref} of 10%

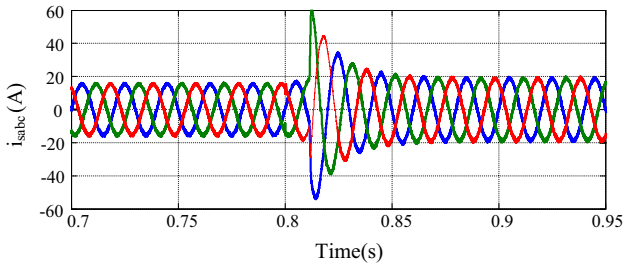

Fig. 17 Waveforms of the grid-side currents i_{sabc} with increasing V_{dcref} of 10%

6.4.2 Step change of the DC bus voltage reference

The dynamic behavior of the proposed combined instantaneous power theory and adaptive exact linearization control applied to SAPF based on multicellular power converter under a step change of V_{dcref} from 1000 to 1100 V (about 10%) is presented in Fig. 16. After a short transient, the DC bus voltage is maintained close to its new reference with a good approximation and stability and without overshot. The grid-side currents have nearly sinusoidal waveforms as illustrated in Fig. 17. The corresponding transient values confirm that the SAPF is stable with a time response of 0.05 s (about 2.5 cycles of the power grid frequency), and the static error is $\varepsilon_s = 3$ V.

6.4.3 Variable nonlinear load power

It aims at comparing the constant DC bus voltage and the adaptive DC bus voltage, for V_{dc}= 1000 V. Figure 18 shows sinusoidal grid currents when $R_L = 40\ \Omega$ and $L_L = 10$ mH. The THD = 4.2% satisfies the limits of IEEE standard. When the nonlinear load is increased to 300% as shown in Fig. 18, grid currents are non-sinusoidal and the THD = 14.77%, i.e., out of IEEE standard.

When V_{dc}= 1400 V, Fig. 19 shows the grid currents when $R_L = 40\ \Omega$ and $L_L = 10$mH, the THD = 12.1% is out of IEEE standard. When the nonlinear load is increased with 300% as shown in Fig. 19, grid currents are sinusoidal and the THD = 3.5% satisfies the limits of IEEE standard.

According to previous results, SAPF with constant DC bus voltage is not suitable for variable nonlinear load.

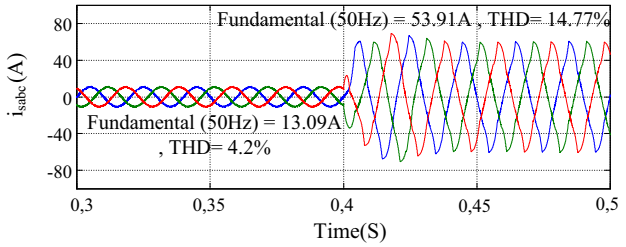

Fig. 18 Waveforms of i_{sabc} with increasing nonlinear load of 300% and V_{dc} = 1000 V

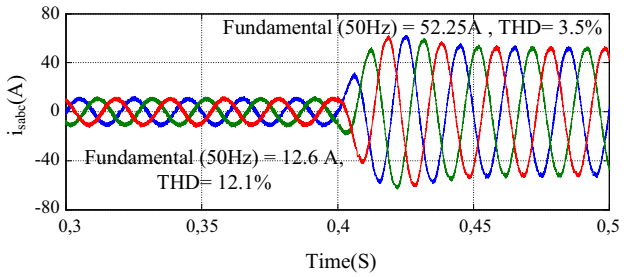

Fig. 19 Waveforms of i_{sabc} with increasing nonlinear load of 300% and V_{dc} = 1400 V

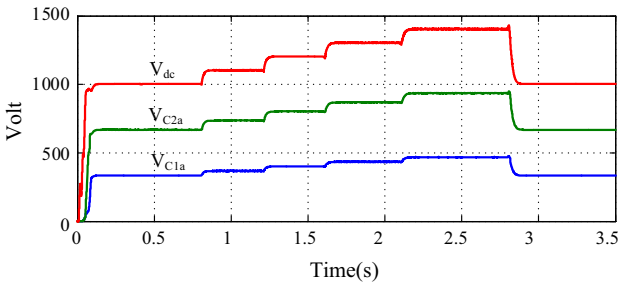

Fig. 20 V_{dc}, V_{C1a} and V_{C2a} with different levels of nonlinear load power

To validate the performance of the proposed control, six perturbations or increase in the nonlinear load power is introduced. In Fig. 20, the DC bus voltage changes adaptively with the nonlinear load power variations to inject the required harmonics. The nonlinear load power is increased by 20%, 50%, 100%, 200%, 400% and finally is decreased with 20% of the initial value at the instants 0.4 s, 0.8 s, 1.2 s, 1.6 s, 2.1 s and 2.8 s, respectively. The adaptive exact linearization control regulates the flying capacitor voltages at their references ($V_{c1ref} = V_{dc}/3$, $V_{c2ref} = 2V_{dc}/3$) and generates the appropriate value V_{dcref} to guarantee a low voltage stress of switches and low switching loss. These conditions are guaranteed because the DC voltage is divided on three cells and achieved a low THD in the grid-side current.

Figures 21 and 22 show the nonlinear load currents and the grid-side currents, respectively. As we can see, the grid-side currents are sinusoidal. According to these figures, the nonlinear load currents have a THD with initial values

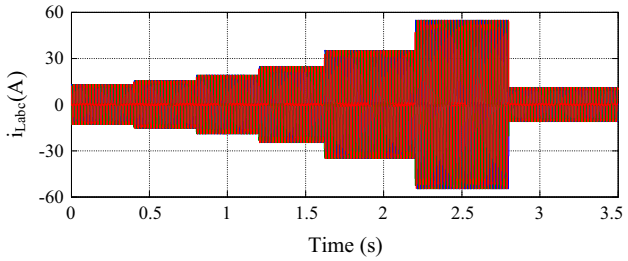

Fig. 21 Waveforms of nonlinear load currents i_{Labc} with different levels of nonlinear load power

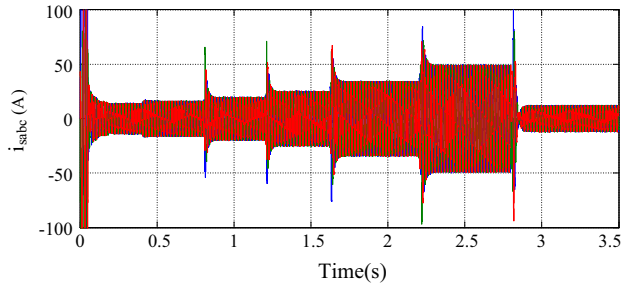

Fig. 22 Waveforms of grid-side current i_{sabc} with different levels of nonlinear load power

Table 3 Simulation results

Simulation time (s)	DC bus voltage V_{dcref} (V)	THD_{iL} of nonlinear load currents (%)	THD_{is} of grid-side currents (%)
0–0.4	1000	23.74	4.35
0.4–0.8	1000	22.97	4.20
0.8–1.2	1100	21.88	3.90
1.2–1.6	1200	20.21	3.85
1.6–2.1	1300	17.21	3.55
2.1–2.8	1400	12.31	3.05
2.8–3.5	1000	24.38	5.01

of 23.74% and the grid-side currents have THD value of 4.35%.

The THD of the grid-side currents, THD of nonlinear load currents and DC bus voltage are summarized in Table 3. These results confirm the improvement of the performances of the adaptive exact linearization control while decreasing the THD of grid-side current for different power levels of nonlinear load connected in the power grid.

In Table 3, when the nonlinear load power increases, the fundamental signal of nonlinear load current i_L increases also, implying a decrease in THD value of i_L. So, it is easier to compensate the THD of grid current by the proposed active power filter. It is the same case between the first and the last values of THD, for which they have the same V_{dcref}, but with different levels of nonlinear load power. As it is shown in Table 3, for the first case, i_L has THD = 23.74% and for the last case THD (i_L) = 24.38%. It is due to the different magnitudes of i_L with the same V_{dcref}. The compensation of harmonics in the first case is easier than in the last case.

7 Conclusion

In this paper, we investigated the design of three-phase shunt active power filter (SAPF) based on four-level multicellular power converter with exact linearization control using the instantaneous power theory. The performance of the proposed design control in different levels of nonlinear load power was verified. The results show that the DC bus voltage regulates adaptively with nonlinear load variation with minor static error, reduces switching loss and guarantees low THD values of grid currents. As further directions, we propose to deal with the fault-tolerant control of active power filter based on multicellular power converter.

References

Ait Chihab, A., Ouadi, H., Giri, F., & El Majdoub, K. (2016). Adaptive backstepping control of three-phase four-wire shunt active power filters for energy quality improvement. *Journal of Control Automation and Electrical Systems, 27*(2), 144–156.

Alexandre, C. M., Luiz, C. P. D., & Helmo, K. M. P. (2018). Power quality study and analysis of different arc welding machines. *Journal of Control Automation and Electrical Systems, 29*(2), 163–176.

Antunes, H. M. A., Silva, S. M., Brandao, D. I., Machado, A. A. P., & de Filho, B. J. C. (2018). Harmonic compensation using a series hybrid filter in a centralized AC microgrid. *Journal of Control Automation and Electrical Systems, 29*(2), 219–229.

Aourir, M., Abouloifa, A., Elotmani, F., Aouadi, C., Hamdoun, A., & Lachkar, I. (2018). Flatness based control of single phase multicellular shunt active power filter for power quality improvement. In *Renewable energies power systems & green inclusive economy (REPS-GIE)*, Casablanca, Morocco, 23th to 24th April, https://doi.org/10.1109/REPSGIE.2018.8488853.

Babaei, E., & Hosseini, S. H. (2009). New cascaded multilevel inverter topology with minimum number of switches. *Energy Conversion and Management, 50*(11), 2761–2767.

Belaidi, R., Haddouche, A., Fathi, M., Larafi, M. M., & Chikouche, A. (2011). Improvement of the electrical energy quality using a Shunt Active Filter supplied by a photovoltaic generator. *Energy Procedia, 6,* 522–530.

Bensaid, R. (2001). Observateur des tensions aux bornes des capacités flottantes pour les convertisseurs multicellulaires séries. PhD thesis, Toulouse France, L'institut national polytechnique de Toulouse.

Bouzelata, Y., Kurt, E., Altın, N., & Chenni, R. (2015). Design and simulation of a solar supplied multifunctional active power filter and a comparative study on the current-detection algorithms. *Renewable and Sustainable Energy Reviews, 43,* 1114–1126.

Chang, G. W., Hong, R.-C., & Su, H.-J. (2013). An efficient reference compensation current strategy of three-phase shunt active power filter implemented with processor-in-the-loop simulation. *International Transactions on Electrical Energy Systems, 24,* 125–140.

Chaoui, A., Gaubert, J. P., & Krim, F. (2010). Power quality improvement using DPC controlled three-phase shunt active filter. *Electric Power Systems Research*. https://doi.org/10.1016/j.epsr.2009.10.020.

Chebabhi, A., Fellah, M. K., Kessal, A., & Benkhoris, M. F. (2016). A new balancing three level three dimensional space vector modulation strategy for three level neutral point clamped four leg inverter based shunt active power filter controlling by nonlinear back stepping controllers. *ISA Transactions, 63,* 328–342.

Chen, F., Chen, Z., Wang, H., & Le, J. (2010). Research of State Exact Feedback Linearization control of shunt single-phase active power filter. In *2010 Asia-Pacific power and energy engineering conference*, https://ieeexplore.ieee.org/document/5449133.

Colak, I., Kabalci, E., & Bayindir, R. (2011). Review of multilevel voltage source inverter topologies and control schemes. *Energy Conversion and Management, 52*(2), 1114–1128.

Defaÿ, F., Llor, A.-M., & Fadel, M. (2008). A predictive control with flying capacitor balancing of a multicell active power filter. *IEEE Transactions on Industrial Electronics, 55*(9), 3212–3220.

Fadel, M., Llor, A. M., Duong Tran, B., & Ziani, A. (2012). Direct control of 4-Leg 4-level flying capacitor converter for an active filtering application. *IFAC Proceedings Volumes, 45*(21), 325–330.

Gateau, G. (1997). Contribution à la commande des convertisseurs multicellulaire série. PhD thesis, Toulouse France, L'institut national polytechnique de Toulouse.

Hoseinpour, A., Barakati, S. M., & Ghazi, R. (2012). Harmonic reduction in wind turbine generators using a Shunt Active Filter based on the proposed modulation technique. *Electrical Power and Energy Systems, 43*(1), 1401–1412.

Kale, M., & Özdemir, E. (2005). Harmonic and reactive power compensation with shunt active power filter under non-ideal mains voltage. *Electric Power Systems Research, 74*(3), 363–370.

Karuppanan, P., & Mahapatra, K. K. (2014). Active harmonic current compensation to enhance power quality. *International Journal of Electrical Power & Energy Systems, 62,* 144–151.

Lam, C.-S., & Wong, M.-C. (2014). Design and control of hybrid active power filters. *Springer Briefs in Electrical and Computer Engineering*. https://doi.org/10.1007/978-3-642-41323-0.

Lee, S. S., & Heng, Y. E. (2017). A voltage level based predictive direct power control for modular multilevel converter. *Electric Power Systems Research, 148,* 97–107.

Litrán, S. P., & Salmerón, P. (2017). Electromagnetic compatibility analysis of a control strategy for a hybrid active filter. *Electric Power Systems Research, 144,* 81–88.

Liu, B., Ding, Z., Zhao, H., & Jin, D. (2014). Active power filter DC bus voltage piecewise reaching law variable structure control. *Journal of Applied Mathematics*. https://doi.org/10.1155/2014/835720.

Mahanty, R., & Kapoor, A. K. (2008). Quasi-passive filter for harmonic filtering. *Electric Power Systems Research, 78*(8), 1456–1465.

Martinez-Rodriguez, P. R., Escobar-Valderrama, G., Sosa-Zuniga, J. M., Vazquez-Guzman, G., & de Mendoza-Mendoza, J. (2017). Analysis and experimental validation of a controller for a single-phase active power filter based on a 3L-NPC topology. *International Transactions on Electrical Energy Systems*. https://doi.org/10.1002/etep.2385.

Mekri, F., Machmoum, M., Ait-Ahmed, N., & Mazari, B. (2010). A comparative study of voltage controllers for series active power filter. *Electric Power Systems Research, 80*(6), 615–626.

Mesbahi, N., Ouari, A., Ould Abdeslam, D., Djamah, T., & Omeiri, A. (2014). Direct power control of shunt active filter using high selectivity filter (HSF) under distorted or unbalanced conditions. *Electric Power Systems Research, 108,* 113–123.

Meynard, T. A., Foch, H., Thomas, P., Courault, J., Jakob, R., & Nahrstaedt, M. (2002). Multicell converters: basic concepts and industry applications. *IEEE Transactions on Industrial Electronics, 49*(5), 955–964.

Olivier, T. (1998) Commande découplante linéaire des convertisseurs multicellulaires séries, modélisation synthèse et expérimentation. Ph.D. thesis, toulouse France, L'institut national polytechnique de Toulouse.

Ouchen, S., Betka, A., Abdeddaim, S., & Menadi, A. (2016). Fuzzy-predictive direct power control implementation of a grid connected photovoltaic system, associated with an active power filter. *Energy Conversion and Management, 122,* 515–525.

Ray, S., Gupta, N., & Gupta, R. A. (2018). Hardware realization of proportional-resonant regulator based advanced current control strategy for cascaded H-bridge inverter based shunt active power filter. *International Transactions on Electrical Energy*. https://doi.org/10.1002/etep.2714.

Roldán-Pérez, J., Zamora-Macho, J. L., Ochoa-Giménez, M., & García-Cerrada, A. (2017). A steady-state harmonic controller for a series compensator with uncertain load dynamics. *Electric Power Systems Research, 150,* 152–161.

Sadigh, A. K., Dargahi, V., & Corzine, K. (2016). Analytical determination of conduction power loss and investigation of switching power loss for modified flying capacitor multicell converters. *IET Power Electronics, 9*(2), 175–187. https://doi.org/10.1049/iet-pel.2015.0369.

Sakar, S., Balci, M. E., Abdel Aleem, S. H. E., & Zobaa, A. F. (2017). Increasing PV hosting capacity in distorted distribution systems using passive harmonic filtering. *Electric Power Systems Research, 148,* 74–86.

Singh, J., Dahiya, R., & Saini, L. M. (2017). Buck converter-based cascaded asymmetrical multilevel inverter with reduced components. *International Transactions on Electrical Energy Systems, 28*(3), 1–17.

Taallah, A., & Mekhilef, S. (2014). Active neutral point clamped converter for equal loss distribution. *IET Power Electronics, 7*(7), 1859–1867.

Wu, J.-C., Jou, H.-L., & Wu, K.-D. (2005). A PWM controlled variable damping resistor for protecting the power capacitor/passive power filter. *Electric Power Systems Research, 73*(1), 9–18.

Yao, J., Yu, M., Hu, W., Chen, Z., & Zhou, T. (2016). Improved control strategies for a DFIG-based wind-power generation system with SGSC under unbalanced and distorted grid voltage conditions. *International Journal of Electrical Power & Energy Systems, 77,* 185–196.

Yu, J., Li, Y., Cao, Y., & Xu, Y. (2018). An impedance-match design scheme for inductively active power filter in distribution networks. *International Journal of Electrical Power & Energy Systems, 99,* 638–649.

Zafari, A., & Jazaeri, M. (2016). A novel structure of hybrid active power filter based on voltage-current source converter (VCSC-HAPF). *International Transactions on Electrical Energy Systems*. https://doi.org/10.1002/etep.2299.

Zhao, W., Luo, A., Peng, K., & Deng, X. (2009). Current control for a shunt hybrid active power filter using recursive integral PI. *Journal of Control Theory and Applications, 7*(1), 77–80.